Available online at www.sciencedirect.com
SCIENCE DIRECT
Catalysis Today 114 (2006) 102–111
CATALYSIS TODAY
www.elsevier.com/locate/cattod

Intra-channel evolution of carbon monoxide and its implication on the regeneration of a monolithic $Pt/K/Al_2O_3$ NO_x storage-reduction catalyst

Jae-Soon Choi [a,*], William P. Partridge [a], William S. Epling [b], Neal W. Currier [b], Thomas M. Yonushonis [b]

[a] *Fuels, Engines, and Emissions Research Center, Oak Ridge National Laboratory, P.O. Box 2008, MS-6472, Oak Ridge, TN 37831–6472, USA*
[b] *Cummins, Inc., 1900 McKinley Avenue, MC 50227, Columbus, IN 47201, USA*

Available online 9 March 2006

Abstract

Understanding how a reductant evolves and is utilized during regeneration of NO_x storage-reduction catalyst can lead to predictive kinetic models, improved catalysts and energy-efficient engine-catalyst systems. We performed practically relevant NO_x storage/regeneration cycling (56 s/4 s) experiments over a monolithic $Pt/K/Al_2O_3$ catalyst in a bench-flow reactor and resolved multiple transient reactions and exotherms. Carbon monoxide was the reductant and intra-channel speciation and temperature measurements were instrumental in resolving CO chemistry. Gas-phase O_2 reacted with CO very fast over the entire regeneration time, and was depleted at the catalyst front. The resulting exotherm was significant and dissipated slowly over time raising the subsequent storage temperature considerably. NO_x release/reduction by CO was also vigorous and primary NO_x removal occurred at early regeneration times. The NO_x-attributable exotherm was smaller than that of the O_2–CO reaction, but extended deeper into the front portion of catalyst due to axially distributed NO_x storage. Secondary NO_x release/reduction occurred after the primary and produced NH_3 as the main product. Hydrogen appeared when and where both the O_2 consumption and major NO_x release/reduction were near complete. We proposed that H_2 produced via water–gas shift (WGS) reaction had little impact on O_2 depletion and primary NO_x release/reduction under the conditions studied. Further study is necessary to assess the impact of WGS reaction on secondary NO_x release/reduction.

Keywords: NO_x storage-reduction catalyst; Lean NO_x trap; NO_x adsorber catalyst; $Pt/K/Al_2O_3$; Monolith; Regeneration; Carbon monoxide; Exotherm; Water–gas shift reaction; Intra-channel measurement

1. Introduction

As planned regulations will mandate drastic reduction in NO_x emissions from diesel engines [1], considerable effort is being made to develop and implement cleaner diesel technology. Among multiple technical options being explored is NO_x storage-reduction (NSR) catalysts which have shown potential in meeting future NO_x emission standards [2]. Also known as lean NO_x traps (LNTs) or NO_x adsorber catalysts (NACs), NSR catalysts combine NO_x storage components (in general, alkali or alkaline-earth metal) with supported precious metals (similar to 3-way catalysts) [3–7]. Under typical lean exhaust conditions, NSR catalysts reversibly store NO_x as nitrates or nitrites (storage step). As the extent of NO_x storage reaches a pre-determined level, the exhaust is made rich to release and reduce the stored NO_x (regeneration step). Lean/rich cycling circumvents the issue of poor NO_x removal efficiency of conventional 3-way catalyst under lean environment. Moreover, HC-SCR have been showing unsatisfactory performance despite much effort to improve their activity, selectivity, and stability [8]. However, periodic regeneration of NSR catalyst by creating rich environment results in extra fuel consumption and requires sophisticated engine-catalyst system control. Successful implementation of NSR technology, with minimum fuel penalty, will require improved catalyst design, optimized system configuration and control strategy, and predictive kinetic model. To this end, more complete understanding of NSR catalysis is necessary, particularly, about

* Corresponding author. Tel.: +1 865 946 1368; fax: +1 865 946 1354.
E-mail address: choijs@ornl.gov (J.-S. Choi).

0920-5861/$ – see front matter © 2006 Elsevier B.V. All rights reserved.
doi:10.1016/j.cattod.2006.02.011

regeneration step, which is much less understood than storage step.

For example, how a reductant evolves and is utilized inside a catalyst channel during regeneration is important missing information in current open literature [3]. In this respect, carbon monoxide is an interesting species to study, as it is a dominant reductant produced from certain engine-managed regeneration strategies [9]. Under practical conditions, CO reductant is expected to interact with various exhaust species in addition to NO_x, such as residual gas-phase O_2 and H_2O. Therefore, reactions such as $CO + NO_x$, $CO + O_2$, $CO + H_2O$ can occur simultaneously and compete. Inherently transient (i.e., fast cycling) and integral (i.e., propagation of the breakthrough front over catalyst) nature of NSR catalyst operation makes its evaluation challenging especially under practically relevant conditions (fast cycling, monolith, high reductant level, high reaction exotherms). Analytical tools with high temporal and spatial resolution are necessary to acquire more detailed kinetic and mechanistic details of NSR catalysis.

In this study, our goal was to resolve multiple reactions and associated exotherms occurring during fast lean/rich cycling experiments over $Pt/K/Al_2O_3$ catalyst with CO reductant and get improved understanding of regeneration step. Well-controlled bench experiments were performed and special emphasis was put on intra-channel speciation and temperature measurements by deploying spatially-resolved capillary-inlet mass spectrometer (SpaciMS) and phosphor thermography (PhosT), respectively. Concerted use of SpaciMS and PhosT made it possible to study dynamic chemistry along the monolith channels as it developed over space and time. Our focus was not on evaluating the effect of different reaction parameters (e.g., temperature, concentration, gas composition), but on capturing important reaction features (e.g., nature and sequence of reactions) based on our transient observations under a chosen set of conditions.

2. Experimental

A $Pt/K/Al_2O_3$/cordierite catalyst was prepared and provided by a catalyst manufacturer (EmeraChem). The substrate was 31 cells per cm^2 Rauschert cordierite monolith. The monolith was dipped into an aqueous slurry containing a high surface area (160 $m^2\ g^{-1}$) alumina. Excess solution was drained, the sample was allowed to dry, and then was calcined for 1 h in ambient air. The platinum and potassium components were then added by incipient wetness methods. First, a proprietary platinum salt dissolved in water was impregnated onto a coated monolith and calcined in ambient air. Potassium was subsequently deposited by using aqueous carbonate solution and the sample was dried in ambient air. For the bench reactor study, a sample was removed from the monolith block by boring out a 2.54 cm-diameter and 7.62 cm-long core.

The core was wrapped in fiber glass insulation tape and inserted into a quartz reactor tube which was enclosed in an electric furnace. The tape eliminates gas bypass around the sample during the experiments. The reactor tube was positioned horizontally in a furnace such that the catalyst core was located towards the outlet end of the reactor tube. All reactant gas lines were preheated to enhance the catalyst temperature uniformity. Gas mixtures were metered using mass-flow controllers, with H_2O introduced into a heated zone using a high-precision liquid metering pump. A rapid switching valve system was used to alternate between the lean and rich gas mixtures (with mixed flows already fully established) so that the lean/rich/lean transitions in these experiments were almost instantaneous. Tables 1–3 list the typical conditions of cycling experiments. The reactor was equipped with a bypass line so that both the entering and exiting gases could be analyzed by MKS FT-IR analyzer.

Table 1
Details of the standard NO_x storage/regeneration cycling experiment

	Storage (lean)	Regeneration (rich)
Duration	56 s	4 s
Space velocity	30000 h^{-1}	30000 h^{-1}
NO	250 ppm	0 ppm
CO	0%	4%
O_2	8%	1%
H_2O	5%	5%
N_2	Balance	Balance

Intra-channel gas phase speciation was performed by using SpaciMS developed in the Fuels, Engines, and Emissions Research Center at Oak Ridge National Laboratory [9–11]. The mass spectrometer, employed in this study had a magnetic-sector mass filter, which allows quantitative measurement of H_2 [12] as well as H_2O, total NO_x, O_2, and CO_2. A minimally invasive capillary inlet system (sampling rate = ca. 10 μL/min, probe size = ca. 185 μm) was employed to transport time-varying species pools to the mass spectrometer for analysis. Capillary probes were introduced from the reactor inlet and positioned at different catalyst locations.

Table 2
Details of the cycling experiment without NO

	Storage (lean)	Regeneration (rich)
Duration	56 s	4 s
Space velocity	30000 h^{-1}	30000 h^{-1}
NO	0 ppm	0 ppm
CO	0%	4%
O_2	1%	1%
H_2O	5%	5%
N_2	Balance	Balance

Table 3
Details of the cycling experiment without NO and O_2

	Storage (lean)	Regeneration (rich)
Duration	56 s	4 s
Space velocity	30000 h^{-1}	30000 h^{-1}
NO	0 ppm	0 ppm
CO	0%	4%
O_2	0%	0%
H_2O	5%	5%
N_2	Balance	Balance

Intra-channel transient temperature distributions were measured using a small optical fiber tipped with a thermographic phosphor. Such phosphor thermography has been described by Allison and Gillies [13]. In general the technique is based on the temperature dependence of a phosphor's excited-state lifetime; in practice, temperature is determined through calibration curves from excited-state lifetime measurements. The minimally invasive nature of the optical-fiber probe is similar to that of the SpaciMS capillary. The motivation for using phosphor thermography was to mitigate probe-attributable conductive broadening and thus enhance the spatial resolution of high thermal gradients; conductive probes spatially broaden parameter gradients just as slow instruments temporally broaden parameter transients. The physical probe was based on a 255 μm OD optical fiber (Fiberguide Ind., SFS200/220/255), tipped with manganese-activated magnesium fluorogermanate, Mg_4FGeO_6:Mn or MFG, phosphor (Osram Type 2363, or Phosphor Technology EQD25/N-U1) using a high-temperature binder (VHT, SP-115); the resulting sensor tip was about 0.2 mm thick and 0.25 mm in diameter. The MFG-tipped fiber probe was butt-coupled to a fiber coupler (200 μm core, RoMack Inc.) for excitation and detection. A nitrogen laser (337 nm, SRS NL100) was coupled into the excitation leg of the fiber coupler and used to excite the MFG. A fraction of the isotropically emitted phosphorescence was captured by the probe fiber, transferred through the fiber-coupler detection leg, filtered through a band-pass filter (650 nm λ_c, 75 nm FWHM, Intor), and detected using a PMT (Hamamatsu, R7400U-01). The time constant of the exponentially decaying PMT signal is proportional to the MFG excited-state lifetime, and in turn the MFG-local temperature. The PMT decay signal was monitored at 400 kH (National Instruments, DAQPad 6070E) through a diode limiter and unity-gain buffer circuits in parallel with a 470 kΩ shunt, and analyzed via LabView. The resulting temperature measurement rate was about 2–4 Hz.

3. Results

To obtain a detailed understanding of NSR-catalyst regeneration under practically relevant conditions, a standard NO_x storage/regeneration fast-cycling experiment was performed (details in Table 1). To facilitate deconvolution of the multiple potential CO reactions (CO + NO; CO + O_2; CO + H_2O), fast cycling experiments were also performed without NO (details in Table 2), as well as in the absence of both NO and O_2 in the feed (details in Table 3). In this study, the ability to monitor CO_2 dynamics with SpaciMS was critical as it permitted to decouple multiple CO reactions indirectly. Therefore, CO_2 was not included in the inlet gas-stream to prevent large background interference, even though the real diesel exhaust contains a high level of CO_2. The intra-catalyst gas composition and reaction temperature were analyzed at different axial locations with high temporal resolution via SpaciMS and PhosT, respectively. SpaciMS probes were placed in 0.75 in. increments within the catalyst: catalyst inlet (0.0 in.), 1/4 position (0.75 in.), 1/2 position (1.5 in.), 3/4 position (2.25 in.) and catalyst outlet (3.0 in.); where 0 in. and 3 in. correspond to the front and back catalyst faces, respectively. PhosT probes were placed in 0.5 in. increment: −0.5 in., 0.0 in., 0.5 in., 1.0 in., 1.5 in., 2.0 in., 2.5 in.. The SpaciMS detected and quantified total NO_x (NO + NO_2, *m/z* 30), H_2 (*m/z* 2), H_2O (*m/z* 18), O_2 (*m/z* 32), and CO_2 (*m/z* 44).

3.1. Standard NO_x storage/regeneration fast cycling experiment

Fig. 1a shows NO_x breakthrough profiles for a representative 56-s storage/4-s regeneration cycle, and provides a global picture of the catalyst performance along the catalyst length. During the storage phase, major NO_x uptake occurred in the first 1/4 of catalyst with some NO_x slip to the downstream locations. The practical totality of the NO_x escaping the first 1/4 was stored in the second 1/4 of catalyst. The extent of storage

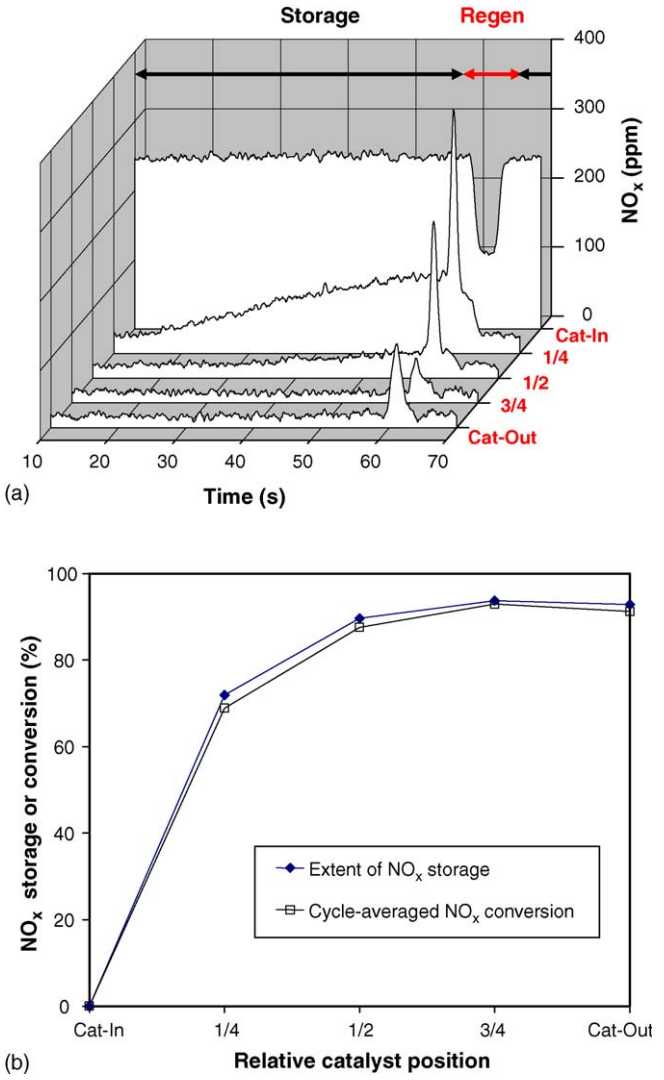

Fig. 1. NO_x removal performance of a 3 in.-long Pt/K/Al_2O_3-washcoated monolith during 54-s storage/4-s regeneration cycling. Storage gas: 250 ppm NO, 8% O_2, 5% H_2O and N_2 balance; regeneration gas: 4% CO, 1% O_2, 5% H_2O and N_2 balance; catalyst mid-bed T = 430 °C. (a) NO_x breakthrough profiles at different axial locations obtained by SpaciMS. (b) Corresponding cycle-averaged NO_x storage extent and NO_x conversion.

was calculated based on the integrated area under the storage-regime curves and is presented in Fig. 1b. Indeed, little change can be seen from the 1/2 catalyst position to catalyst outlet, with a maximum storage extent of ca. 94%. Residual NO_x of 15–20 ppm passed through the second 1/2 of the catalyst without measurable storage (Fig. 1a), which amounted to 6% NO_x slip from the catalyst (Fig. 1b). However, there is uncertainty on the exact NO_x-slip level during storage, since the estimated NO_x detection limit of the SpaciMS was 20 ppm in this study.

Upon switching to the regeneration gas stream, a NO_x pulse appeared over the first 2 s of the 4-s regeneration (Figs. 1a and 2a). The amplitude of this pulse was largest at 1/4 position and decreased continually until 3/4 position. A slight increase was observed from 3/4 position to cat-out (Figs. 1a and 2a). NO_x pulse is often reported to occur at early regeneration times [11,14,15]. Cycle-averaged NO_x conversion based on SpaciMS analysis is presented in Fig. 1b with a maximum conversion of ca. 93% (cf. 94% maximum storage). Catalyst-outlet FT-IR data (Fig. 2b) were also used to evaluate cycle-averaged performance (Table 4) complementing the SpaciMS analysis. Due to the relatively long residence time of analyzed gas inside the IR-cell, temporal broadening of FT-IR signal was significant (Fig. 2b) compared to SpaciMS data (Fig. 2a); however, this broadening does not affect the accuracy of conversion analysis based on temporal integration. The FT-IR enabled detection of N_2O, NH_3, and CO; measurement of these species with SpaciMS was not possible due to some combination of electron-ionization efficiency and/or relative abundance issues (i.e., interference with other species of much higher intensity CO_2, H_2O, and N_2, respectively). Moreover, NO–NO_2 partitioning can be resolved via FT-IR, whereas SpaciMS measures only total NO_x. The FT-IR data indicate that NO_2 was almost absent and N_2O formation was very small, while non-negligible quantities of NH_3 were produced during regeneration (Fig. 2b). In terms of breakthrough timing, NO and N_2O appeared at regeneration inception, whereas CO and NH_3 were absent at early regeneration times and began evolving later in time. NH_3 breakthrough started slightly later than CO. The cycle-averaged NO_x conversion determined via FT-IR (Table 4) was in good agreement with the SpaciMS-based determination (Fig. 1b). The estimated N_2 selectivity was about 93%. As N_2 was used as the balance gas, direct quantification of N_2 as a product of NO_x reduction was difficult. Thus, N_2 selectivity was calculated based on total NO_x converted and N_2O and NH_3 produced.

Table 4
Cycle-averaged catalyst performance data based on FT-IR gas analysis at reactor outlet

Criteria	%
CO conversion	95.3
NO_x conversion	97.9
N_2O selectivity[a]	0.4
NH_3 selectivity[a]	6.9
N_2 selectivity[b]	92.7

[a] With respect to total NO_x converted.
[b] Calculated assuming that N_2O and NH_3 are only by-products.

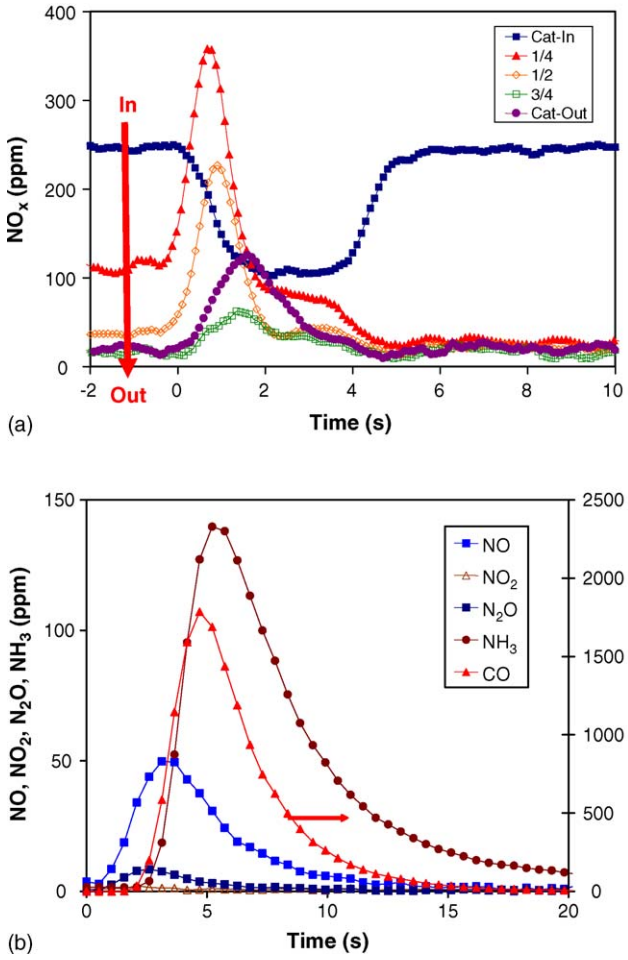

Fig. 2. (a) Spatially resolved NO_x breakthrough profiles and (b) catalyst-outlet gas composition measured by FT-IR during regeneration of a 3 in.-long Pt/K/Al_2O_3-washcoated monolith. Storage gas: 250 ppm NO, 8% O_2, 5% H_2O and N_2 balance; regeneration gas: 4% CO, 1% O_2, 5% H_2O and N_2 balance; catalyst mid-bed T = 430 °C.

Fig. 3 presents O_2, CO_2, H_2, and H_2O profiles obtained by SpaciMS at different axial locations just before, during, and just after catalyst regeneration. The cat-in O_2 curve indicates a distinct shift in the O_2 level from 8 to 1% as the inlet gas stream was switched from storage to regeneration (Fig. 3a). Small CO_2 could be seen at this cat-in position due to gas-phase CO oxidation by O_2. Oxygen was absent in the gas stream from the 1/4 to cat-out positions over the entire regeneration period, suggesting very efficient CO + O_2 reaction. A correspondingly large amount of CO_2 was produced within the first 1/4 catalyst, with smaller subsequent increases observed from 1/4 to cat-out positions (Fig. 3a). CO_2 profiles were asymmetric, with an increasing portion of the leading edge missing at greater depths into the catalyst; similarly, the CO_2 tail at early storage times was increasingly significant for greater catalyst depths (Fig. 3a). It indicates surface adsorption of CO_2 formed by CO + O_2 reaction during regeneration and desorption during subsequent storage. At early regeneration times, H_2 was not observed over the entire catalyst length, while the H_2O level increased along the catalyst (Fig. 3b). At later regen times, however, the water–gas shift (WGS) reaction occurred as

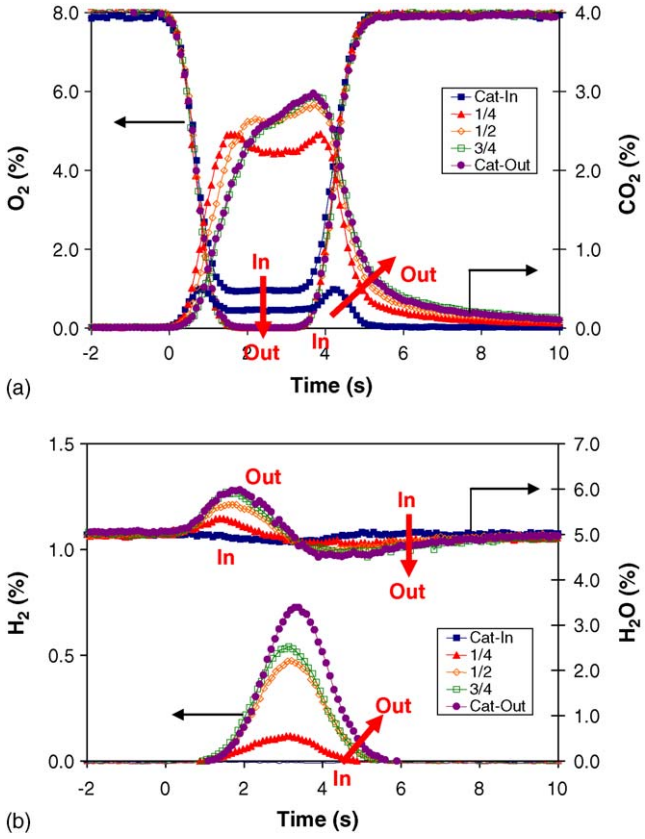

Fig. 3. Spatially resolved breakthrough profiles just before, during, and just after regeneration of a 3 in.-long Pt/K/Al_2O_3-washcoated monolith: (a) O_2 and CO_2 and (b) H_2 and H_2O. Storage gas: 250 ppm NO, 8% O_2, 5% H_2O and N_2 balance; regeneration gas: 4% CO, 1% O_2, 5% H_2O and N_2 balance; catalyst mid-bed $T = 430$ °C.

indicated by H_2 generation and H_2O consumption (Fig. 3b). The CO conversion due to WGS reaction was estimated to be 9% at the cat-out position based on the measured H_2 production.

Fig. 4 shows temperature profiles at different axial locations measured by PhosT for reactor operation as defined in Table 1.

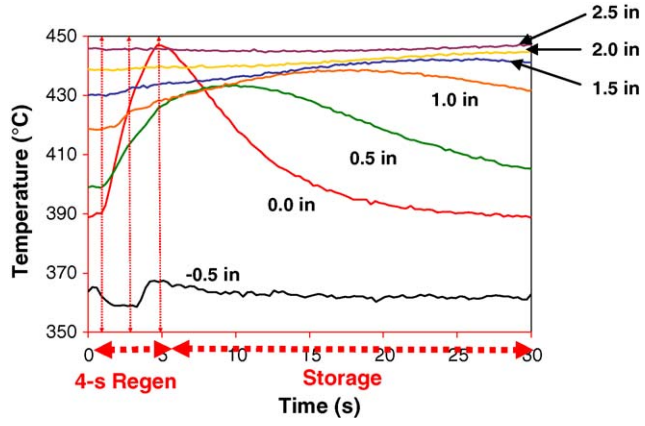

Fig. 4. Temperature profiles at different axial locations obtained by phosphor thermography during 54-s storage/4-s regeneration cycling over a 3 in.-long Pt/K/Al_2O_3-washcoated monolith. Storage gas: 250 ppm NO, 8% O_2, 5% H_2O and N_2 balance; regeneration gas: 4% CO, 1% O_2, 5% H_2O and N_2 balance; catalyst mid-bed $T = 430$ °C.

The experimental setup used in this study produced a ~ 50 °C temperature gradient across the catalyst length, with 430 °C at 1/2 position (1.5 in.) in the absence of reaction exotherm (see Fig. 4 at 0 s). The inlet gas temperature of the regeneration gas pool was lower than the storage gas stream as indicated in Fig. 4 by the −0.5 in. position (0.5 in. before the catalyst inlet) curve. However, as will be shown later via temperature profiles for the case without NO and O_2 in the feed, this inlet temperature difference disappeared by the 0.0 in. (cat-in) position (apparently due to the heat capacity of the catalyst monolith); i.e., in the absence of CO reactions with NO and O_2, the cat-in temperature profile is flat over the NSR cycle. Thus, any temperature change observed inside the catalyst may be interpreted as resulting from heats of reactions. Thus, in Fig. 4 high-frequency intra-catalyst temperature dynamics are attributable to exothermic reactions, while low-frequency dynamics are indicative of bulk heat transfer.

At regeneration inception, a large exotherm was produced at the catalyst face (0.0 in. curve in Fig. 4). The maximum of this exotherm (at catalyst face) is synchronous with the end of regeneration, indicating active exothermic reaction(s) throughout regeneration. The timing of the temperature maximum was increasingly delayed from regen inception with increasing depth into the catalyst. Similarly, the amplitude of the temperature dynamic decreased with increasing depth into the catalyst. The slow heat dissipation led to considerably higher temperatures during the subsequent storage phase, compared to the baseline case without exothermic reactions. A close look at the catalyst-face temperature transient reveals the existence of two distinct exotherms: a distinct slope change is apparent at about the regeneration-period mid point. The data indicates that one strongly exothermic reaction was spatially confined to the catalyst front but occurred over the full regeneration times. A second weaker exothermic reaction of shorter duration occurred at early regeneration times and was sustained deeper into the catalyst. The combination of the two exothermic reactions produces a greater slope at early-regen times at the catalyst-front locations. Indeed, the common slope-changing time (at ~ mid regeneration) for the 0.0 in., 0.5 in. and 1.0 in. catalyst positions indicates termination of a temporally short spatially distributed exothermic reaction.

3.2. Fast cycling experiment without NO in the feed

Oxygen depletion by CO was very efficient in the absence of feed NO, and completed within the first 1/4 of the catalyst (Fig. 5a). Accordingly, a large amount of CO_2 was formed inside the first 1/4 of the catalyst. Some minor gas-phase oxidation of CO took place at cat-in location prior to the catalyst. Again, the CO_2 profiles were asymmetrically biased to late regen times, with long tails extending to the next storage. The magnitude of the missing and tailing CO_2 in Fig. 5a at early-regen and early-storage times, respectively, was similar to that observed in Fig. 3a. In the absence of gas-phase O_2, CO_2 production was much slower over the 1/4 to cat-out positions. Hydrogen production via WGS reaction increased considerably (Fig. 5b) compared to the experiment with NO in the feed

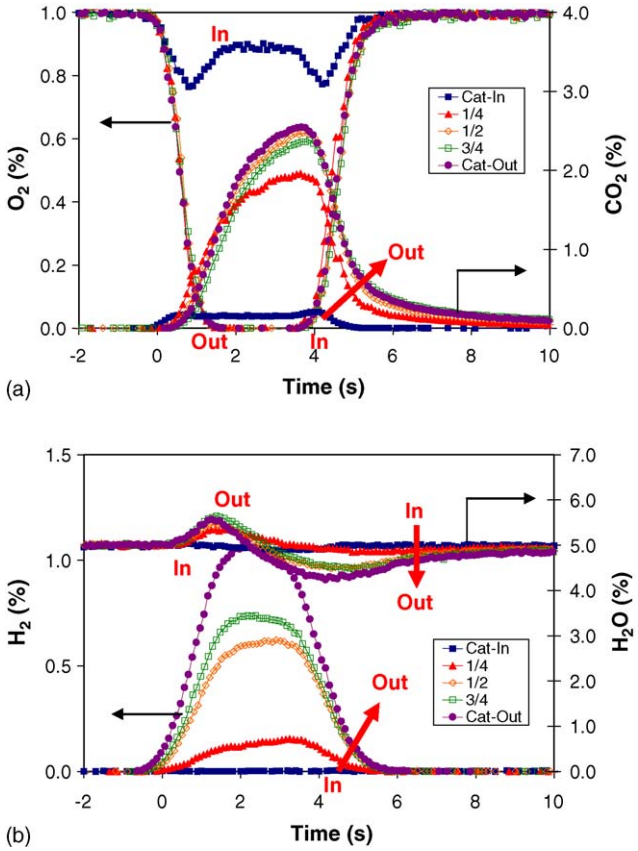

Fig. 5. Spatially resolved breakthrough profiles just before, during, and just after regeneration of a 3 in.-long Pt/K/Al_2O_3-washcoated monolith: (a) O_2 and CO_2 and (b) H_2 and H_2O. Storage gas: 0 ppm NO, 1% O_2, 5% H_2O and N_2 balance; regeneration gas: 4% CO, 1% O_2, 5% H_2O and N_2 balance; catalyst mid-bed $T = 430$ °C.

(Fig. 3b). At the 1/4 position, H_2 began to evolve slightly after regeneration inception; the delay from regeneration inception of H_2-evolution onset monotonically diminished with increasing depth into the catalyst, with the cat-out H_2-evolution and regeneration inceptions being synchronous. The CO conversion due to WGS reaction was estimated to be 22% based on H_2 production. At early regeneration times, H_2O increased (Fig. 5b) as in the case of NO in the feed (Fig. 3b). However, contrary to the case with NO feed, early-regeneration H_2O production was notably less significant beyond the 1/4-catalyst position. Moreover, late-regeneration H_2O consumption was greater without NO feed (Fig. 5b) compared to the case with NO feed (Fig. 3b). The H_2O production–consumption balance point, at which time the water concentration was equal to the inlet value, occurred at increasingly early regeneration times at distances deeper into the catalyst (Fig. 5b).

A large exotherm, similar to that with NO feed (Fig. 4), was observed at the catalyst face (Fig. 6). The exotherm maximum coincided with regeneration termination. The evolving pattern of the exotherm maxima in terms of temporal location and amplitude indicates slow dissipation of heat produced at the catalyst face during regeneration. The transient temperature distributions without NO did not show the distinct additional exotherm at early regeneration times which was observed in the case with NO feed (Fig. 4).

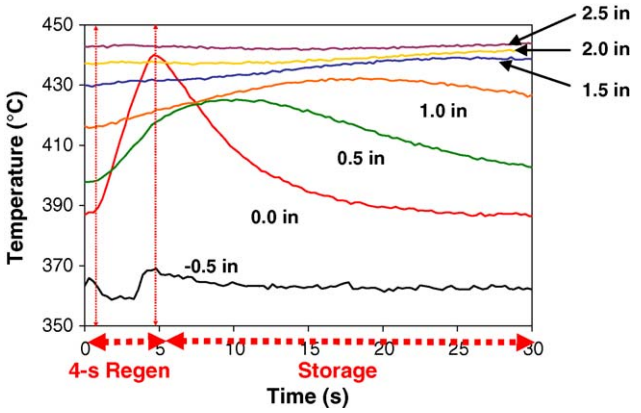

Fig. 6. Temperature profiles at different axial locations obtained by phosphor thermography during 54-s storage/4-s regeneration cycling over a 3 in.-long Pt/K/Al_2O_3-washcoated monolith. Storage gas: 0 ppm NO, 1% O_2, 5% H_2O and N_2 balance; regeneration gas: 4% CO, 1% O_2, 5% H_2O and N_2 balance; catalyst mid-bed $T = 430$ °C.

3.3. Fast cycling experiment without NO and O_2 in the feed

In this case, CO_2 evolution was much smaller and more progressive along the catalyst (Fig. 7a) compared to the previous two cases (Figs. 3a and 5a). As with the previous two cases, the CO_2 profiles were asymmetrically biased to late

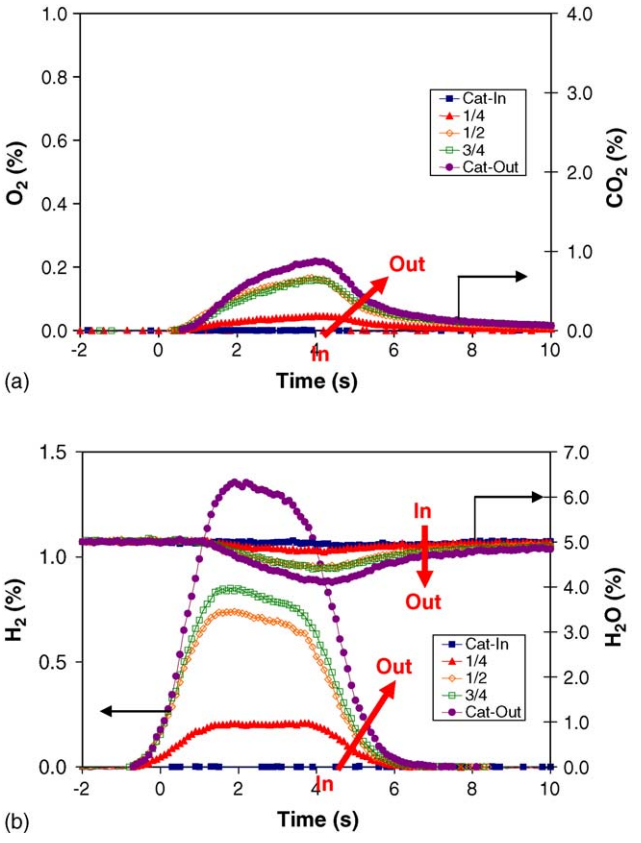

Fig. 7. Spatially resolved breakthrough profiles just before, during, and just after regeneration of a 3 in.-long Pt/K/Al_2O_3-washcoated monolith: (a) O_2 and CO_2 and (b) H_2 and H_2O. Storage gas: 0 ppm NO, 0% O_2, 5% H_2O and N_2 balance; regeneration gas: 4% CO, 0% O_2, 5% H_2O and N_2 balance; catalyst mid-bed $T = 430$ °C.

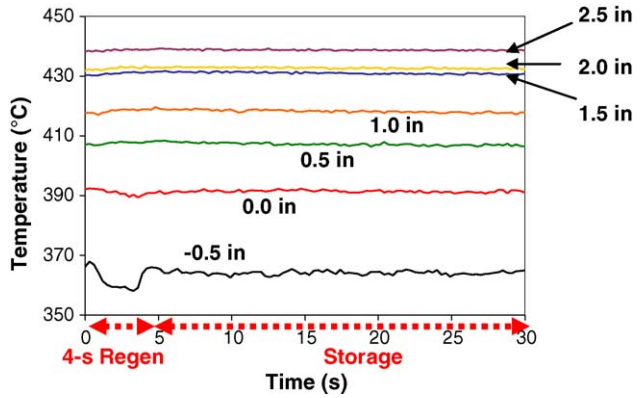

Fig. 8. Temperature profiles at different axial locations obtained by phosphor thermography during 54-s storage/4-s regeneration cycling over a 3 in.-long Pt/K/Al_2O_3-washcoated monolith. Storage gas: 0 ppm NO, 0% O_2, 5% H_2O and N_2 balance; regeneration gas: 4% CO, 0% O_2, 5% H_2O and N_2 balance; catalyst mid-bed $T = 430$ °C.

regen times and displayed long tails, with both features becoming more pronounced through the catalyst. Hydrogen production via WGS reaction started readily at regeneration inception at every catalyst position including 1/4 position (Fig. 7b). The estimated cat-out CO conversion due to WGS reaction was 33%. Contrary to the cases with O_2 and both O_2 and NO in the feed, H_2O production was not observed at early regeneration times (Fig. 7b). Instead, the H_2O level was constant at the feed value for the first 1 s or so before starting to decrease. H_2O consumption increased through the catalyst and mirrored H_2 production.

The temperature profiles show that no significant exotherms were produced during regeneration for this case (Fig. 8). As mentioned before, the temperature difference between regeneration and storage gas streams observed before the catalyst (−0.5 in.), was absent over the entire catalyst.

4. Discussion

4.1. Overall performance of Pt/K/Al_2O_3 during NO_x storage/regeneration cycling

The amount of CO introduced during the 4-s regeneration was about 40% more than what would be necessary to reduce all the stored NO_x and gas-phase O_2 with a stoichiometry of $CO/O_2 = 2$ and $CO/NO_x = 2.4$. Such a CO/NO_x stoichiometry was determined previously over the same catalyst under the conditions where gas-phase O_2 was absent and the CO + H_2O reaction and formation of N_2O and NH_3 were limited [11]. Both SpaciMS (Fig. 1) and FT-IR analyses (Table 4) indicated that near complete NO_x removal was achieved in this study by using only the front 1/2 of catalyst for NO_x storage (Fig. 1). Moreover, O_2 was depleted inside the first 1/4 (Fig. 3a). The cycle-averaged CO conversion was over 95% at catalyst outlet (Table 4), which was 35% more than the amount necessary to reduce all the stored NO_x and O_2 based on the abovementioned stoichiometry. This "extra" CO consumption can be explained by participation of the WGS (Fig. 3b) and NH_3 formation (Fig. 2b) reactions. In addition, it is reasonable that some additional CO consumption occurred due to surface oxygen removal in the second 1/2 of catalyst where practically no NO_x was stored. Near 93% N_2 selectivity was achieved with NH_3 as the main by-product of NO_x reduction.

4.2. Nature and sequence of reactions occurring during NSR catalyst regeneration with CO reductant

As mentioned above, the SpaciMS data demonstrated gas-phase O_2 depletion within the first 1/4 of catalyst both with and without NO_x storeage prior to the regeneration step (Figs. 3a and 5a). The PhosT measurements indicated that O_2 depletion was achieved even before the 1/4 position (Figs. 4 and 6). Indeed, if we compare the temperature profile at the 0.0 in. position of Fig. 4 with that of Fig. 6, it is clear that the CO + O_2 reaction produced the large exotherm whose maximum coincided with regeneration termination and that this reaction did not produce significant exotherm any more at 0.5 in. position. This indicates that O_2 depletion was near complete even at 0.5 in. (1/6-cat) position. The synchronous timing of the catalyst-face temperature maximum and regeneration termination is in accordance with O_2 depletion by CO over the entire regeneration period (Figs. 3a and 4). Recently, the researchers at the University of Houston have observed similarly high exotherms during cycling operation of a Pt/Ba/Al_2O_3 monolithic catalyst with propylene as a reductant [16]. Five percent of O_2 was present in the inlet gas stream of both lean and rich phases and the catalyst temperature was measured at the mid-point of the monolith with a thermocouple. The reported temperature profile shows a large broad exotherm due to $C_3H_6 + O_2$ reaction and its slow dissipation. These results are consistent with our observation except that our PhosT measurements have resolved two distinct exotherms in lieu of just one. It is not clear at this point if this difference comes from using two different temperature measurement tools or experimental conditions (reductant type, concentrations, catalyst formulation, etc.). In a separate study, they have developed a kinetic model based on their experimental observations [17]. The intra-channel temperature dynamics predicted by their model are, qualitatively, in good agreement with our results obtained by PhosT measurements. However, as they assumed that the heat of NO_x reduction is negligible, the resulting model predicted a single broad exotherm due to C_3H_6 oxidation.

Logically, the smaller exotherm observed at early regeneration times in Fig. 4 and missing in Fig. 6 was due to CO + NO_x reaction. The axially extended nature of this exotherm is consistent with the axial distribution of stored NO_x. The NO_x-attributable exotherm existed only over early regeneration times (∼ first 2 s), contrary to the CO + O_2 reaction exotherm (entire 4 s). Associating the PhosT and SpaciMS measurement, the temporal and spatial location of NO_x release/reduction can be deduced. In fact, SpaciMS NO_x profiles (Fig. 2a) alone indicate only the timing of total NO_x slip; corresponding N_2, NO, NO_2, N_2O, and NH_3 data are necessary to determine the exact timing of NO_x release/reduction. Unfortunately, SpaciMS could not quantify those species under the conditions used in

this study and FT-IR could measure only catalyst-outlet composition with low temporal resolution. However, from the temporal coincidence of the NO_x-attributable exotherm (Fig. 4) and the NO_x slip distributions (Fig. 2a), it is clear that SpaciMS NO_x profiles indicate actual timing of NO_x release/reduction for the case studied. Moreover, the spatial confinement of the NO_x-attributable exotherm to within the 1.5 in. position (Fig. 4), is consistent with near exclusive NO_x storage within the first 1/2 (Fig. 1). A small amount of NO_x escaped the first catalyst 1/2 during regeneration and was removed inside the second catalyst 1/2 (Fig. 2a). It is noteworthy that the NO_x slip pulses during regeneration appeared slightly later at the 3/4 and cat-out positions than they did at the cat-in and 1/4 positions. This temporal delay might have been due to readsorption of NO_x in the second catalyst 1/2. The FT-IR data (Fig. 2b) indicates that CO was completely absent at early regeneration times, while NO slip appeared readily at regeneration inception. Therefore, even though the amount of CO introduced was in stoichiometric excess when time-averaged over the entire regeneration period, the regeneration stream might have been in a CO-deficit condition at early regeneration times. Such a situation could lead to incomplete removal of the above-mentioned ''readsorbed'' NO_x in the second catalyst 1/2 and slightly time delay the corresponding NO_x slip profiles. In summary, NO_x release/reduction was highly efficient and the ''primary'' NO_x release/reduction was completed at early regeneration times inside the first 1/2 of catalyst. Here we use the term ''primary'' to indicate that not all the stored NO_x was removed at early regeneration times. In fact, some portion of NO_x was still being removed from the catalyst at late regeneration times, as indicated by late NH_3 appearance (Fig. 2b). Although FT-IR signal broadening makes exact sequencing of events difficult, it is clear that NH_3 appeared later than NO, N_2O and CO breakthrough. It appears that two distinct NO_x release/reduction schemes were involved during regeneration and we enumerate their respective features as follows:

(i) ''Primary'' release/reduction: occurred at early regeneration times; treated major portion of NO_x; small NO slip probably due to limited CO supply; produced N_2 as major reduction product.
(ii) ''Secondary'' release/reduction: occurred after primary release/reduction; minor portion of NO_x; no NO slip; occurred in CO excess; produced NH_3 as major reduction product.

Further studies are necessary to understand the underlying mechanisms responsible for these two distinct NO_x release/reduction features. For example, we need to confirm the earlier N_2 formation compared to NH_3 by direct N_2 measurement. Such a N_2-NH_3 sequence has been reported previously, however, over Ba- [18–20] and K-based [20] catalysts with pure H_2 [18,19], pure CO [19], and mixture of H_2 + CO [19,20], which seems to support our assumption that N_2 is the main product of the ''primary'' NO_x release/reduction.

On the other hand, more experimental data will be necessary to elucidate underlying mechanisms of NH_3 formation with pure CO as reductant. Recently, Lesage et al. proposed an NCO pathway to explain NH_3 formation over Ba-based NSR catalyst [19]. They observed by FT-IR surface isocyanates species (NCO) and gas-phase NH_3 formation during regeneration. According to their explanation, NH_3 is produced from hydrolysis of NCO surface intermediates, which are formed during NO_x release/reduction by CO. They reported surface NCO species formation on K-based catalyst in a separate paper [20]. However, further study is necessary to conclusively demonstrate NCO to be a precursor to NH_3 formation and not a spectator. In addition to the NCO pathway, we could also envisage NH_3 formation through NO_x reduction by H_2, the latter being provided by WGS reaction. Indeed, our results show that the regeneration stream was in CO excess (Fig. 2b) and that the WGS reaction occurred at late regeneration times when and where the ''secondary'' NO_x release/reduction occurred (see late H_2 production and H_2O consumption in Fig. 3b). NH_3 formation with pure H_2 reductant has been reported for Ba-based catalysts [18,19,21]. For example, Castoldi et al. have studied $Pt/Ba/Al_2O_3$ catalysts with different Ba-loadings and found that NH_3 is formed at Ba-loading higher than 16% [18]. Interestingly, according to their work, the amount of NH_3 increases with increasing Ba-loading and the temporal overlapping of earlier N_2 peak and later NH_3 peak increases also [18].

4.3. Impact of WGS reaction on NSR catalyst regeneration

Evidence of WGS reaction over NSR catalysts has been reported previously and used mainly to explain catalyst desulfation behavior [22–24]. However, it is still not clear if and how H_2 produced by WGS reaction impacts NSR catalyst regeneration. As described above, H_2 was formed through the WGS reaction at late regeneration times (Fig. 3b) and therefore H_2 might have been used as a reductant for ''secondary'' NO_x release/reduction. As no H_2 was detected at early regeneration times, it appears that WGS reaction was not occurring during primary NO_x release/reduction. Alternatively, WGS reaction could occur at early regeneration times also but immediate consumption by O_2 and NO_x could prevent H_2 detection. This ''intermediate'' WGS reaction scenario appears unlikely for several reasons. First, the WGS reaction is a relatively slow process. For example, in the present study it produced only 33% CO conversion over the entire length of catalyst and in the absence of NO and O_2 in the feed (Fig. 7b); i.e., the most WGS-favorable condition studied. In great contrast, both the CO + O_2 and primary NO_x release/reduction reactions were much faster processes and used a much smaller catalyst length for reaction completion compared to the WGS reaction (Figs. 2 and 3). Moreover, the amount of O_2 and NO_x removed in the first catalyst 1/2 was consistent with total CO consumption at early regeneration times (Fig. 2b). It is therefore likely that O_2 depletion and primary NO_x release/reduction dominated CO consumption when O_2, NO_x and H_2O were in competition for limited CO. The upstream reaction exotherms would have had little impact on WGS reaction at early regeneration times (i.e., no significant rate enhancement), because, as mentioned before, the

heat transfer was relatively slow and even the resulting front edge temperature did not exceed the catalyst mid-bed temperature (Fig. 4). The second observations opposing the ''intermediate'' WGS reaction scenario is based on the dependence of the H_2O profiles evolution on the presence/absence of NO and O_2 in the feed. In the absence of both NO and O_2, CO reacted first with surface H_2O adsorbed during the preceding storage step. This resulted in the initial absence of apparent H_2O consumption matching H_2 production (Fig. 7b). It is revealing that by adding O_2 (Fig. 5b) and NO + O_2 (Fig. 3b) to the feed, the H_2O level increased at early regeneration times. The initial H_2O generation coincided with CO_2 adsorption (Figs. 3 and 5). For example, CO_2 adsorption occurred up to the 3/4 position in the presence of NO + O_2 as did H_2O generation (Fig. 3). Thus, it appears that CO_2 produced by fast CO + O_2 and CO + NO_x reduction displaced surface H_2O, which could not be consumed by the slower WGS reaction. In the case of O_2 alone (Fig. 5), H_2O generation was more spatially confined to the front of the catalyst compared to the case with both NO + O_2; i.e., the initial H_2O generation pulse does not grow as significantly. In this case, the O_2 + CO reaction was almost complete at 0.5 in. position and consequently surface H_2O could be consumed by WGS reaction instead of being displaced by CO_2 at greater depths into the catalyst. Finally, it is unlikely that the observed initial H_2O production resulted from O_2 and NO_x reacting with H_2 produced via WGS reaction because there is no consistent correspondence between the missing H_2 and the corresponding H_2O increase (difference between Fig. 7b and Fig. 3b or Fig. 5b). For example, it follows from the discussion above that CO was depleted at early regeneration times inside the first 1/2 of catalyst considering the amount of O_2 and NO_x removed. Consequently, no WGS reaction could occur in the second catalyst 1/2. However, the initial H_2O generation further increased between the 1/2 and 3/4 positions (Fig. 3b), and therefore this increase was due to surface H_2O displacement by CO_2. In summary, the WGS reaction appears not to play an important role for O_2 depletion and the primary NO_x due to its relatively slow rate. On the contrary, H_2 produced via WGS reaction might participate in the secondary NO_x release/reduction at late regeneration times. Further work will be necessary to assess more quantitatively the issue of surface H_2O displacement by CO_2 and to evaluate the role of H_2 produced by WGS reaction in the secondary NO_x release/reduction.

5. Conclusions

We have temporally and spatially resolved multiple transient reactions and exotherms associated with the regeneration step of a monolithic Pt/K/Al_2O_3 NO_x storage-reduction catalyst during practically relevant fast cycling operation at 430 °C catalyst mid-bed temperature. The obtained results provide improved understanding of regeneration with CO reductant:

- Gas-phase O_2 reacts with CO very efficiently over the entire 4-s regeneration period. Only a small front portion of the monolith is necessary for O_2 depletion leaving the downstream monolith O_2-free.
- Depletion of gas-phase O_2 results in a large exotherm at the monolith front end, which dissipates slowly over time. This slow heat dissipation significantly raises the subsequent storage-phase temperature.
- Primary NO_x release/reduction is vigorous and occurs at early regeneration times with small NO and N_2O slip.
- Secondary NO_x release/reduction takes place at later regeneration times with NH_3 as the main product.
- The exotherm due to primary NO_x–CO reaction is smaller than that due to O_2–CO reaction, but produced over a greater front portion of the catalyst due to axially distributed NO_x storage.
- The studied catalyst is active in water–gas-shift reaction. CO reacts first with surface H_2O adsorbed during the preceding storage before consuming gas-phase H_2O. However, it appears that WGS reaction is not active during O_2 depletion and primary NO_x release/reduction due to the relatively slow rate of WGS relative to competing CO reactions. Apparently suppressed WGS reaction is accompanied by the displacement of ''pre-adsorbed'' surface H_2O by CO_2 produced by O_2 depletion and the primary NO_x-release/reduction reactions.
- Apparent temperature rise due to WGS reaction is insignificant.
- Further work is necessary to assess the impact of WGS reaction on secondary NO_x release/reduction.

Acknowledgements

The authors are grateful to Jim Lucas and Heather Eadler at Cummins for help in the data collection process. This research was sponsored by the U.S. Department of Energy, Office of FreedomCAR and Vehicle Technologies, with Gurpreet Singh, Ken Howden and Kevin Stork as the Program Managers.

References

[1] U.S. EPA, Federal Register 66 (2001) 5001.
[2] R.C. Yu, A.S. Cole, B.J. Stroia, S.C. Huang, K. Howden, S. Chalk, SAE Technical Paper 2002–01–1867 (2002).
[3] W.S. Epling, L.E. Campbell, A. Yezerets, N.W. Currier, J.E. Parks II, Catal. Rev. -Sci. Eng. 46 (2004) 163.
[4] N. Miyoshi, S. Matsumoto, K. Katoh, T. Tanaka, J. Harada, N. Takahashi, K. Yokota, M. Sugiura, K. Kasahara, SAE Technical Paper 950809 (1995).
[5] N. Takahashi, H. Shinjoh, T. Iijima, T. Suzuki, K. Yamazaki, K. Yokota, H. Suzuki, N. Miyoshi, S. Matsumoto, T. Tanizawa, T. Tanaka, S. Tateishi, K. Kasahara, Catal. Today 27 (1996) 63.
[6] M. Takeuchi, S. Matsumoto, Top. Catal. 28 (2004) 151.
[7] L.J. Gill, P.G. Blakeman, M.V. Twigg, A.P. Walker, Top. Catal. 28 (2004) 157.
[8] R. Burch, J.P. Breen, F.C. Meunier, Appl. Catal. B 39 (2002) 283.
[9] B.H. West, S.P. Huff, J.E. Parks, S.A. Lewis, J.-S. Choi, W.P. Partridge, and J.M. Storey, SAE Technical Paper 2004–01–3023 (2004).
[10] W.P. Partridge, J.M.E. Storey, S.A. Lewis, R.W. Smithwick, G.L. DeVault, M.J. Cunningham, N.W. Currier, T.M. Yonushonis, SAE Technical Paper 2000–01–2952 (2000).
[11] J.-S. Choi, W.P. Partridge, C.S. Daw, Appl. Catal. A. 293 (2005) 24.
[12] T. Collier, C. Burgess, M. Brogan, B. Campbell, A. Finch, K. Reavell, SAE Technical Paper 2004–01–0592 (2004).
[13] S.W. Allison, G.T. Gillies, Rev. Sci. Instrum. 68 (1997) 2615.
[14] E. Fridell, M. Skoglundh, B. Westerberg, S. Johansson, G. Smedler, J. Catal. 183 (1999) 196.

[15] W.S. Epling, G.C. Campbell, J.E. Parks, Catal. Lett. 90 (2003) 45.
[16] K.S. Kabin, R.L. Muncrief, M.P. Harold, Catal. Today 96 (2004) 79.
[17] M. Sharma, M.P. Harold, V. Balakotaiah, Ind. Eng. Chem. Res. 44 (2005) 6264.
[18] L. Castoldi, I. Nova, L. Lietti, P. Forzatti, Catal. Today 96 (2004) 43.
[19] T. Lesage, C. Verrier, P. Bazin, J. Saussey, M. Daturi, Phys. Chem. Chem. Phys. 5 (2003) 4435.
[20] T. Lesage, C. Verrier, P. Bazin, J. Saussey, S. Malo, C. Hedouin, G. Blanchard, M. Daturi, Top. Catal. 30/31 (2004) 31.
[21] H. Abdulhamid, E. Fridell, M. Skoglundh, Top. Catal. 30/31 (2004) 161.
[22] J. Li, J. Theis, W. Chun, C. Goralski, R. Kudla, J. Ura, W. Watkins, M. Chattha, R. Hurley, SAE Technical Paper 2001–01–2503 (2001).
[23] J.R. Theis, J.J. Li, J.A. Ura, R.G. Hurley, SAE Technical Paper 2002–01–0733 (2002).
[24] D.R. Monroe, W. Li, SAE Technical Paper 2002–01–2886 (2002).